J Electroceram (2007) 19:165–182
DOI 10.1007/s10832-007-9043-4

Advances in energy harvesting using low profile piezoelectric transducers

Shashank Priya

Received: 31 May 2006 / Accepted: 8 September 2006 / Published online: 14 March 2007

Abstract The vast reduction in the size and power consumption of sensors and CMOS circuitry has led to a focused research effort on the on-board power sources which can replace the batteries. The concern with batteries has been that they must always be charged before use. Similarly, the sensors and data acquisition components in distributed networks require centralized energy sources for their operation. In some applications such as sensors for structural health monitoring in remote locations, geographically inaccessible temperature or humidity sensors, the battery charging or replacement operations can be tedious and expensive. Logically, the emphasis in such cases has been on developing the on-site generators that can transform any available form of energy at the location into electrical energy. Piezoelectric energy harvesting has emerged as one of the prime methods for transforming mechanical energy into electric energy. This review article provides a comprehensive coverage of the recent developments in the area of piezoelectric energy harvesting using low profile transducers and provides the results for various energy harvesting prototype devices. A brief discussion is also presented on the selection of the piezoelectric materials for on and off resonance applications. Analytical models reported in literature to describe the efficiency and power magnitude of the energy harvesting process are analyzed.

Keywords Piezoelectric · Energy harvesting · Macro fiber composite · PVDF · PZT · Transducer · Bimorph · Windmill

S. Priya (✉)
Materials Science and Engineering, Automation and Robotics Research Institute, The University of Texas,
Arlington, TX 76019, USA
e-mail: spriya@uta.edu

1 Introduction

Energy recovery from wasted or unused power has been a topic of discussion in recent times. Unused power exists in various forms such as industrial machines, human activity, vehicles, structures and environment sources. Among these, some of the promising sources for recovering energy are periodic vibrations generated by rotating machinery or engines. Table 1 lists some of the energy sources available in the surrounding which are/can be tapped for generating electricity. Primarily, the selection of the energy harvester as compared to other alternatives such as battery depends on two main factors cost effectiveness and reliability. In recent years, several energy harvesting approaches have been proposed using solar, thermoelectric, electromagnetic, piezoelectric, and capacitive schemes which can be simply classified in two categories (1) power harvesting for sensor networks using MEMS/thin/thick film approach, and (2) power harvesting for electronic devices using bulk approach. This review article covers the later category in detail using piezoelectric scheme citing examples from literature and authors own work. A brief discussion on the first category is provided in the last section of the article.

Table 2 lists the daily average power consumption for a wearable device with three functions music player, personal organizer, and GSM communication, for three user profiles: intensive (24/24 h), typical (16/24 h and moderate use of the device), and low (8/24 h) [1]. The last row in the table corresponds to the condition if Bluetooth instead of GSM mobile phone is used for communications. It can be seen from this table that a power of 50 mW is required to run the three functions intensively. Table 3 provides the list of power requirement for various household electronic devices. The small portable FM radio or walkman requires a small power level of 30 and 60 mW. These magnitudes of

Table 1 Sources of energy available in the surrounding which are/can be tapped for generating electricity.

Human body	Vehicles	Structures	Industrial	Environment
Breathing, blood pressure, exhalation, body heat	Aircraft, UAV, helicopter, automobiles, trains	Bridges, roads, tunnels, farm house structures	Motors, compressors, chillers, pumps, fans	Wind, solar, temperature gradient, daily temperature
Walking, arm motion, finger motion, jogging, swimming, eating, talking	Tires, tracks, peddles, brakes, shock absorbers, turbines	Control-switch, HVAC systems, ducts, cleaners, etc.	Conveyors, cutting and dicing, vibrating mach.	Ocean currents, acoustic waves, EM waves, RF signal

power are possible to be continuously harvested from human and industrial activity.

A large network with several sensor nodes and data acquisition components requires a centralized energy source that has to be charged or replaced over time. In remote applications such as structural health monitoring of aircrafts or ships, recharging, battery replacement or wiring can be very tedious and expensive task. In many other cases, these operations may be prohibited by the infrastructure. Further, in order for the sensor nodes to be conveniently placed and used they should be as small as possible which puts an upper limit on their life time. If an electronic device with a 1 cm^3 of non-rechargeable lithium battery (at max energy density of 2,880 J/cm^3 or 800 Wh/l) were to consume 100 μW of power on average, the device would last 333 days. A lifetime of approximately 1 year is not practical. Even though the nodes in the wireless network will be much smaller than the 1 cm^3 area, the power requirements will force them to use a battery of much larger size enhancing the system volume [2–8].

There are four possible ways to realize a distributed sensor network with adequate performance as following (1) enhance the energy density of the storage systems (2) reduce the power consumption of the sensor, (3) develop self-powered sensors by generating or harvesting energy or (4) transmit the power from a centralized source to the sensor. Out of these various possible solutions the most efficient and practical method is to develop self-powered sensors by harvesting energy from the wasted energy. Practically, on-site small scale successful harvesting of electrical energy from the available energy source (as listed in Table 1) can solve various challenges and enable new applications.

Figure 1 compares the various alternatives for power sources. The comparison is made using the experimental values available in literature and the data measured in our laboratory [1–14]. The outside solar energy has the capability of providing power density of 15,000 $\mu W/cm^3$ which is about two orders of magnitudes higher than other sources. Definitely, solar energy is a very attractive source for powering sensor networks and the solar technology has matured over the years. One of the major challenges in the implementation of solar technology on "energy on demand" platforms has been the requirement of bulky electronics. Further, the variation in light intensity (cloudy vs. sunny day) can drop the efficiency significantly. Also, the solar power drops down significantly inside the building. The other most attractive source is kinetic energy comprising of mechanical vibrations, air flow and human power. The kinetic energy can be converted into electric energy using piezoelectric, electromagnetic or electrostatic mechanism. It can be easily shown that piezoelectric transducers are more suitable as kinetic to electrical energy converters. In addition to the advantage of being smaller and lighter the piezoelectrics have three times higher energy density as

Table 2 The daily average power consumption for a wearable device with three functions.

	Profile (24 h)		
Function	Low	Typical	Intensive
Shutdown	33.33% (8 h)	33.33% (8 h)	0% (0 h)
MP3	4.16% (1 h)	16.66% (4 h)	25% (6 h)
Organizer	2.08% (0.5 h)	4.16% (1 h)	8.33% (2 h)
Communications	2.08% (0.5 h)	4.16% (1 h)	25% (6 h)
Standby	58.33% (14 h)	41.66% (10 h)	41.66% (10 h)
Average Power	17.7 mW	37 mW	110 mW
Energy in a day	1529 J	3197 J	9507 J
Average Power Bluetooth Comm.	12.5 mW	26.5 mW	48.5 mW

Based on-Shutdown 100 μW; MP3 110 mW; Organizer 50 mW; Communication 300 mW; Standby 10 mW.

Table 3 Average power consumption of common household devices.

Product	Average power consumption
Small portable FM radio	30 mW
Walkman (play mode)	60 mW
TV remote	100 mW
Cell phone (talk/stand-by)	2 W/35 mW
Electric torch (flashlight)	4 W
Video 8 (no LCD screen)	6 W
Laptop computer	10 W
TV (53/67/wide screen)	50/74/11 W

compared to their counterparts electrostatic and electromagnetics. Figure 2 compares the magnitude of the energy density for the three types of converters. In this figure, the symbol ε is the dielectric constant, E is the electric field, B is the magnetization, X is the stress, d is the piezoelectric strain constant and g is the piezoelectric voltage constant [15].

The general principle for conversion of mechanical low frequency AC stress into electrical energy using a piezoelectric transducer is shown schematically in Fig. 3. This transformation from mechanical to electrical energy is obtained through the direct piezoelectric effect and using a rectifier and DC–DC converter circuit the generated electrical energy is stored. There are three primary steps in power generation as outlined in this schematic: (a) trapping the mechanical AC stress from available source, (b) converting the mechanical energy into electrical energy with piezoelectric transducer and (c) processing and storing the generated electrical energy. The mechanical output can be in the form of a burst or continuous signal depending on the cyclic mechanical amplifier assembly. Depending on the frequency and amplitude of the mechanical stress one can design the required transducer, its dimensions, vibration mode and desired piezoelectric material. The energy generated is proportional to frequency and strain and higher energy can be obtained by operating at the resonance.

2 Analysis of vibration to electric conversion

Williams and Yates have proposed a generalized model for the conversion of the vibration energy into electrical energy as shown in Fig. 4 [16]. The model assumes that the mass of the vibration source is much greater than the seismic mass in the generator, and that the vibration source is an infinite source of power. The differential equation of motion describing the system in terms of the housing vibration ($y(t)=Y_o\cos\omega t$) and relative motion of mass ($z(t)$) is given as:

$$m\ddot{z}(t) + d\dot{z}(t) + kz(t) = -m\ddot{y}(t) \tag{1}$$

Where m is the seismic mass, d is the damping constant and k is the spring constant. The total power dissipated in the damper under sinusoidal excitation was found to be given as [17]:

$$P(\omega) = \frac{m\varsigma Y_o^2 \left(\frac{\omega}{\omega_n}\right)^3 \omega^3}{\left[1-\left(\frac{\omega}{\omega_n}\right)^2\right]^2 + \left[2\varsigma\left(\frac{\omega}{\omega_n}\right)\right]^2} \tag{2}$$

where, $\omega_n^2 = k/m$ is the system resonant frequency and $\varsigma = d/2\sqrt{mk}$ is the damping ratio. If the vibration spectrum is known beforehand than the device can be tuned to operate at the resonance frequency of the system, in which case the maximum power that can be generated is given as:

$$P_{\max} = \frac{mY_o^2\omega_n^3}{4\varsigma} \tag{3}$$

Equation 3 implies that the power is inversely proportional to the damping ratio which should be minimized through

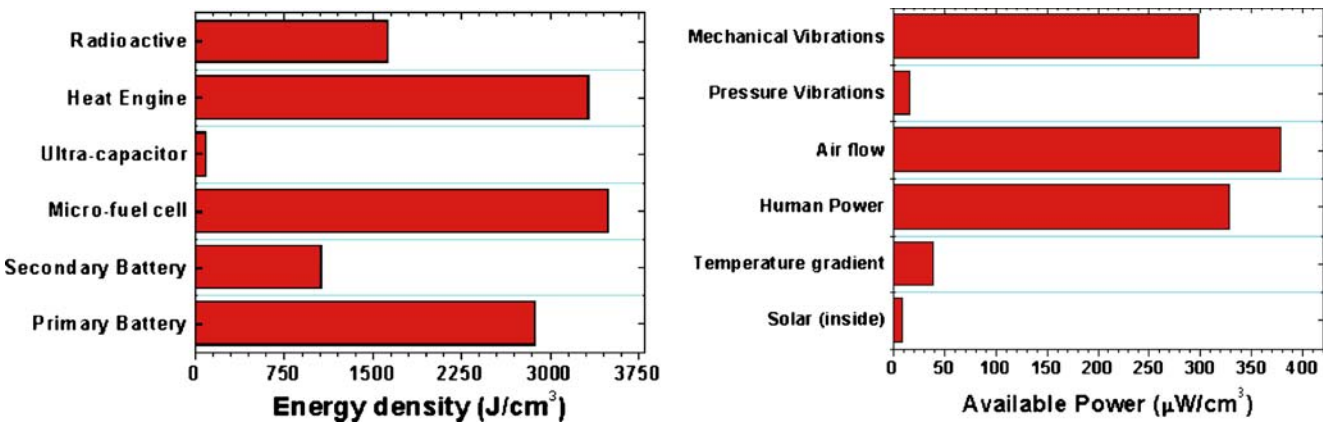

Fig. 1 Comparison of various potential power sources for the sensor networks [7, 14, 18, 26]

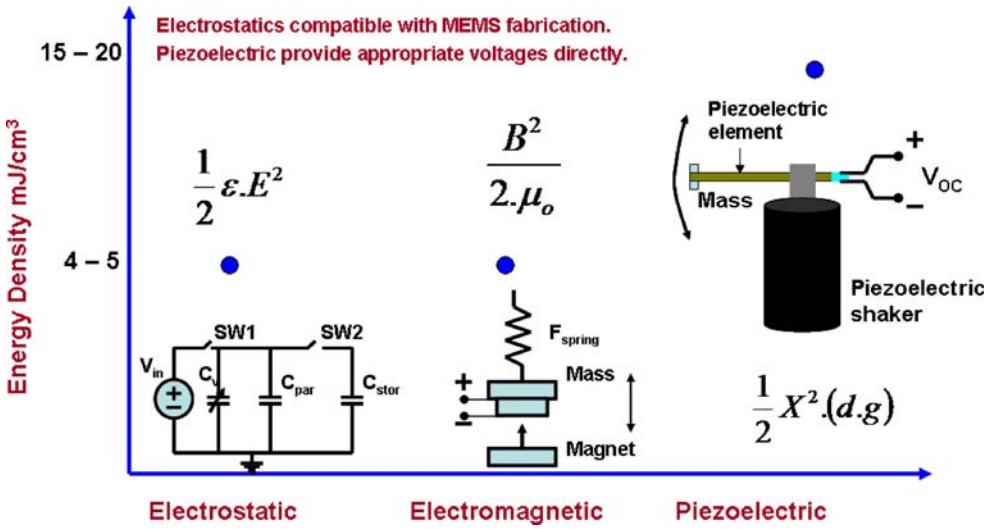

Fig. 2 Comparison of the energy density for the three types of mechanical to electrical energy converters

proper selection of the materials and design. The loss factor (roughly equal to 2ς) for some commonly used structural materials are quite small, e.g., aluminum ~0.007 and steel ~0.05. In terms of the acceleration the above expression can be written as:

$$P_{\max} = \frac{m\alpha^2}{4\omega_n \varsigma} \tag{4}$$

which implies that output power is proportional to the square of the acceleration. Another important conclusion that can be drawn from Eq. 4 is that output power is directly proportional to the proof mass of the system and thus reducing the size of the converter reduces the conversion efficiency. Table 4 provides a list of acceleration and peak frequency values for the common vibration sources [7]. It has been found that accelerations of 2.5 m/s^2 at 120 Hz are typical of many low level vibrations. Figure 5 shows the example of a vibration spectrum from a car driven at 65 mph and washing machine. In this figure the spectral peaks at 1.2, 14 and 35 Hz correspond to fundamental frequency, structural imbalance, and engine speed (http://www.vibrationdata.com/).

The power generated by the converter is measured across the electrical load. In order to analyze the frequency response of the electromechanical system it is easier to perform the analysis using the equivalent circuit model. Table 5 lists the analogy between the mechanical and electrical parameters that can be used to derive the equivalent circuit for a given mechanical system [18]. The dimension of mechanical impedance is same as that of mechanical resistance and is expressed in the same unit, N·s/m, often defined as mechanical ohms. Figure 6 shows the electrical equivalent circuit of the vibration source and elastic load. These equivalence relations can be used in analyzing the performance of the system.

In the off-resonance condition the modeling of the generator can be significantly simplified as illustrated in Fig. 7. Figure 7a shows the schematic of the piezoelectric bimorph transducer of height H, length L and width W subjected to the AC force F. The load dependence of the bimorph in the frequency range far from the resonance can be computed by using the equivalent circuit representation shown in Fig. 7b. In this circuit the voltage source is taken to be the open circuit voltage across the bimorph. The voltage across the load can than be expressed as [19]:

$$V_{\text{Load}} = V_{OC}\left|\frac{R_{\text{Load}}}{R_{\text{Load}} + \frac{1}{j\omega C} + R_s}\right| \tag{5}$$

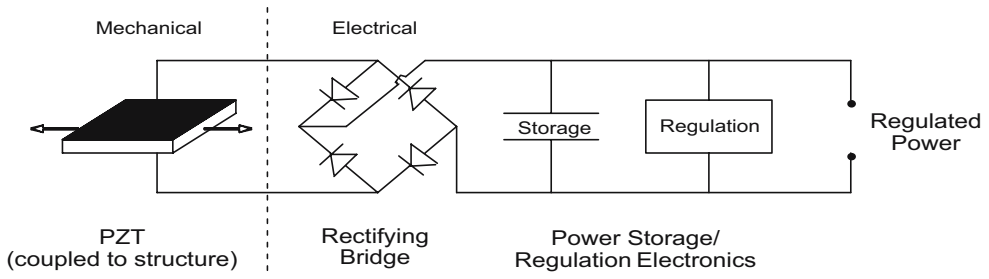

Fig. 3 Schematic representation of the piezoelectric energy harvesting

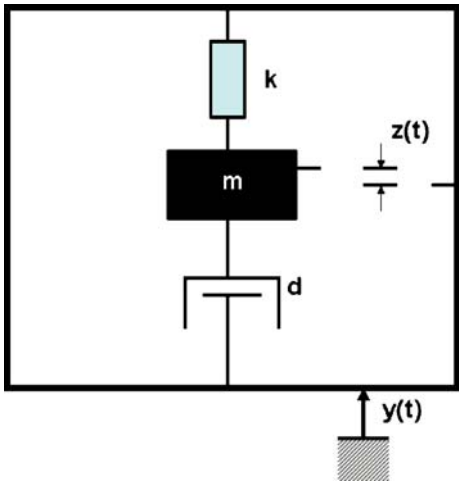

Fig. 4 Schematic of the piezoelectric generator

where R_s is the series resistance $\left(R_s = \frac{\tan\delta}{2\pi f\, C}\right)$ and C is the damped capacitance of the bimorph.The average power delivered to the load can than be found using the expression:

$$P = \frac{V_{\text{Load}}^2}{2R_{\text{Load}}} \tag{6}$$

The power reaches maximum at an optimum load $\left(R_{\text{Load}}^{\text{opt}}\right)$ which for the equivalent circuit shown in Fig. 7b is given as:

$$R_{\text{Load}}^{\text{opt}} = \left|R_s + \frac{1}{j\omega C}\right| \tag{7}$$

At resonance the piezoelectric generator is generally represented as an LCR circuit consisting of motional elements (L_A, C_A, and R) in parallel to the damped capacitance, C_d. The elements L_A and C_A represent the piezoelectric response while R_A represents the combined effect of resistances associated with the dielectric loss R_d (damped) and the mechanical loss R_m (motional). The reactive equivalent circuit components for a rectangular plate operating in the 31 mode are given by the following expressions [20]:

$$L_A = \left[\frac{\sigma}{8}\right]\left[\frac{lb}{w}\right]\left[\frac{s_{11}^{E^2}}{d_{31}^2}\right] \tag{8}$$

$$C_A = \left[\frac{8}{\pi^2}\right]\left[\frac{lw}{b}\right]\left[\frac{d_{31}^2}{s_{11}^E}\right] \tag{9}$$

where l is the length and w is the width of the rectangular plate, s is the elastic compliance and d is the piezoelectric constant. A rigorous analysis for the piezoelectric bimorph loaded in cantilever form with the tip mass m has been conducted by Roundy et al.. They used the transformer based equivalent circuit for the analysis and arrived at the following expression have for the off-resonance and resonance conditions [7, 9]:

$$P = \frac{1}{2R}\frac{\left(\frac{2k_{31}t_c}{k_2}\right)^2\frac{c_p}{\varepsilon}A_m^2}{\left[\frac{\omega_n^2}{\omega RC_b} - \omega\left(\frac{1}{RC_b} + 2\varsigma\omega_n\right)\right]^2 + \left[\omega_n^2\left(1+k_{31}^2\right) + \left(\frac{2\varsigma\omega_n}{RC_b}\right) - \omega^2\right]^2}$$

$$(\text{off} - \text{resonance}) \tag{10}$$

$$P = \frac{m^2}{2k}\frac{RC_b^2\left(\frac{2k_{31}t_c}{k_2}\right)^2\frac{c_p}{\varepsilon}A_m^2}{\left(4\varsigma^2 + k_{31}^4\right)(RC_b)^2k + 4\varsigma k_{31}^2RC_b\sqrt{km} + 4\varsigma^2m} \tag{11}$$

$$(\text{resonance})$$

where c_p is the elastic constant of the piezoelectric ceramic, k_{31} is the piezoelectric coupling coefficient, t_c is the thickness of one layer of the piezoelectric ceramic, k_2 is a geometric constant that relates average piezoelectric material strain to the tip deflection, ε is the dielectric constant of piezoelectric material, R is the load resistance and C_b is the capacitance of the piezoelectric bimorph. This equation also leads to the same conclusion as Eq. 2 that maximum power is obtained by operating at the resonance frequency.

The resonance frequency of the piezoelectric transducer is dependent upon the configuration, size, and loading conditions. Figure 8 exemplifies the size dependence of the resonance frequency for circular unimorphs (1 layer of PZT) and bimorphs (2 layer of PZT) operating in radial mode. The material variables in this figure are diameter of the metal and PZT discs. The diameter of the PZT disc is 2.5 mm smaller than the metal disc diameter. It is evident from this figure that the resonance frequency changes by one order of magnitude by increasing the disc diameters by about four times for unimorphs. Another common method of lowering the resonance frequency is by adding more piezoelectric layers to the piezoelectric transducer called as "multimorph." In addition to lowering the resonance frequency of the structure multimorph transducer provides

Table 4 Peak acceleration and frequency of common structures.

Vibration Source	Peak acceleration (m/s^2)	Frequency of peak (Hz)
Base of a 5 HP 3-axis machine tool	10	70
Notebook computer while CD is being read	0.6	75
Clothes dryer	3.5	120
Second story floor of a wood frame office building	0.2	100

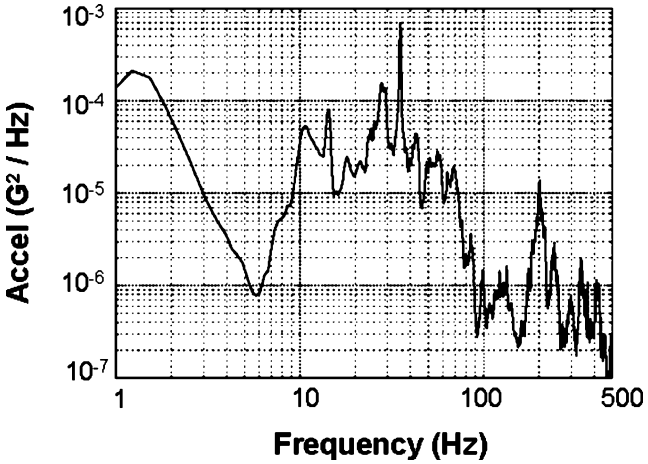

Fig. 5 Power spectral density of the car (2003 Ford Taurus) driven on highway at 65 mph. The data was recorded using Nicolet Vision System. (Source: Website—http://www.vibrationdata.com. Permission granted by T. Irvine to reproduce the figure). The spectral peak at 1.2 Hz is the fundamental frequency of the vehicle mass and suspension system and is typical for passenger cars. Other peaks can be associated to the tire imbalance, engine vibrations, and rotational vibrations from drive train system, alternator, and air conditioning unit

higher charge output. For example—a rectangular bimorph of the dimension $60\times35\times0.6$ mm^3 mounted in cantilever fashion and operating in bending mode has the resonance frequency of 65 Hz. By adding four additional layers to this bimorph the resonance frequency can be lowered to 45 Hz [21]. An multimorph (more than six layers) of size $24\times6\times0.3$ mm^3 can sense an acceleration frequency of as low as 0.5 Hz [22]. Results on accelerometer devices have shown that by increasing the number of layers from six to 12 the charge output is increased by 30% [22].

3 Energy conversion efficiency

The efficiency of the vibration to electric energy conversion process is dependent upon the method of applying the oscillating stress onto the piezoelectric and material parameters. Umeda et al. have analyzed the electric energy generation from the piezoelectric diaphragm structure which is vibrated by dropping a steel ball (d_{31} mode) [23, 24]. The impact of the steel ball induced vibration in the piezoelectric diaphragm resulting in AC voltage. Their

Table 5 Analogy between the electrical and mechanical parameters.

Mechanical Parameter [unit]	Electrical parameter
Force [N]	Voltage [V]
Velocity [m/s]	Current [A]
Mass [kg]	Inductance [H]
Compliance [m/N]	Capacitance [F]
Damping [Ns/m]	Resistance [Ω]

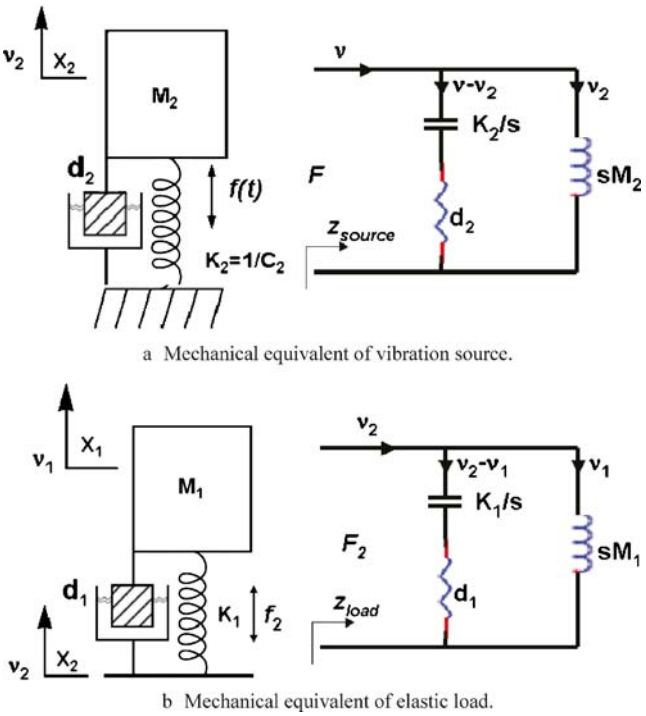

Fig. 6 Electrical equivalence of the mechanical system for vibration source and elastic load representing the relationship shown in Table 5 (adopted from: Permission granted by H. Kim to reproduce the figure). The unit of mechanical impedance is similar to resistance and is given as N s/m

analysis revealed that large part of the impact energy was returned to the steel ball in the form of kinetic energy causing it to bounce off the plate. In case the steel ball did not bounce off rather vibrated with the piezoelectric diaphragm the efficiency of the system was computed to

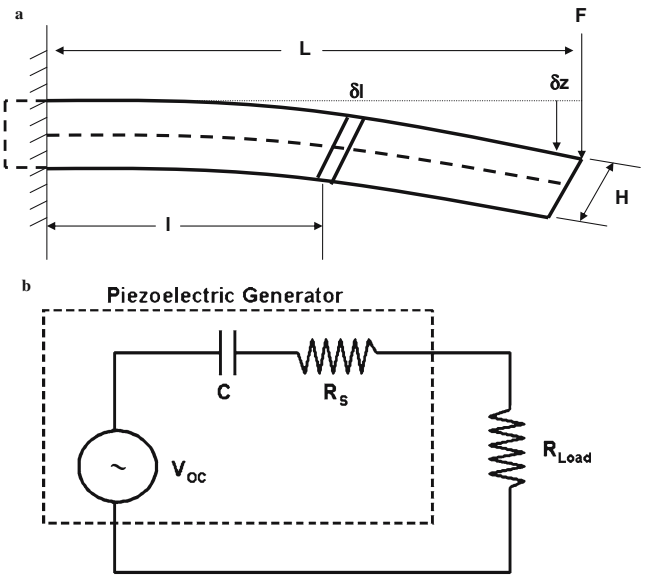

Fig. 7 Schematic of the model for the piezoelectric bimorph. **a** Strain in a bent rectangular section cantilever for width w and thickness H. **b** Equivalent circuit representation of the piezoelectric generator in off-resonance condition

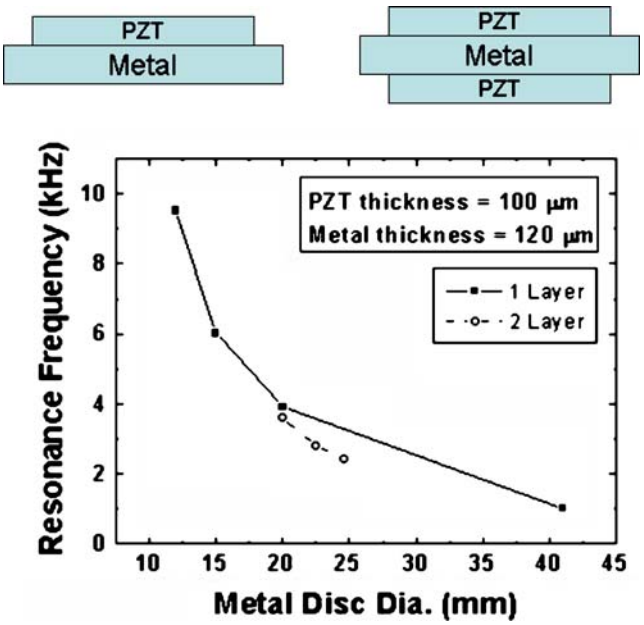

Fig. 8 Variation of the resonance frequency for the unimorph and bimorph as a function of the diameter

be 52%. Further, the study showed that the efficiency increased with the increase in mechanical quality factor (Q_m), coupling factor (k) and decrease in dielectric loss factor ($\tan\delta_d$) [23, 25, 26].

Goldfarb and Jones investigated the electric energy generation from stack actuators under the cyclic forced condition (d_{33} mode) [27]. It was pointed out that the problem associated with the piezoelectric converters is the fact that they store the large fraction of the energy produced and return it to the excitation source. Thus, the efficiency of the system can be improved by minimizing the energy stored in the piezoelectric material. The maximum efficiency was found at the frequency of 5 Hz and the efficiency became negligible above 100 Hz which clearly indicates the frequency sensitive nature of stacks. Funasaka et al. have made a comparison of the performance of $LiNbO_3$ and PZT cantilevers for the converter [28]. It was found that $LiNbO_3$ performed better than PZT due to higher coupling and mechanical quality factor.

Recently a quantitative model for the energy conversion efficiency was developed which provides a method for evaluating the material and transducer design in the resonance condition [27]. The model assumes that a rigid mass is coupled to a stationary surface through a spring, damper and piezoelectric element poled along the thickness direction. An oscillating force is applied on the rigid mass which exerts the stress on the piezoelectric converting the mechanical energy into electric energy. The efficiency (η) of the conversion process in this case was found to be given by the relation [29]:

$$\eta = \left(\frac{1}{2}\right)\frac{k^2}{1-k^2}\Big/\left(\frac{1}{Q_m}+\frac{1}{2}\frac{k^2}{1-k^2}\right) \tag{12}$$

Based on this model it was found that by increasing the effective mass by a factor of 2 leads to an 8% increase in the efficiency while decreasing the damping by a factor of 2 results in a 17% increase in the efficiency. The coupling factor is related to the equivalent circuit parameters and hence the materials constants by the relation:

$$k^2 = \left(1 + {}^{C_d}/_{C_A}\right)^{-1} \tag{13}$$

The mechanical quality factor Q_m (=1/tanδ_m) is related to the dielectric loss (tanδ_d) and other piezoelectric material parameters by the following expression (assuming 31 mode operation) [30]:

$$Q_m^{-1} = \frac{\tan\delta_d\left(\pi\varepsilon_0\varepsilon_{33}^T g_{31}^2\right)}{s_{11}^D + \pi\varepsilon_0\varepsilon_{33}^T g_{31}^2} \tag{14}$$

where s_{11}^D is the elastic compliance under constant electric field and g_{31} is the piezoelectric voltage constant. This equation indicates that losses play an important role in efficiency of the process since a significant increase in the dielectric loss will reduce Q_m dramatically. Equations 12, 13, 14 can be used in approximating the efficiency of the generator. For example if an efficiency of 85% is desired than there are several combinations of k^2 and Q_m possible from Eq. 12 such as k^2=0.1 and Q_m=100 [29]. These numbers can than be used to select the piezoelectric material with relevant piezoelectric constants. The selection of the device structure is dependent upon various factors such as dimensions, fabrication technique, and cost effectiveness.

The choice of the material in the off-resonance condition is dependent on the ability of the piezoelectric to convert applied stress into dielectric charge effectively, which is related to the piezoelectric voltage constant (g).

4 Piezoelectric material selection in off-resonance condition

At low frequencies far from the resonance a piezoelectric plate can be assumed to behave like a parallel plate capacitor. Hence, electric energy available under ac stress excitation is given as [31, 32]:

$$U = \frac{1}{2}CV^2 \quad \text{or} \quad \text{energy per unit volume},$$
$$u = \frac{1}{2}(\text{d.g})\cdot\left(\frac{F}{A}\right)^2 \tag{15}$$

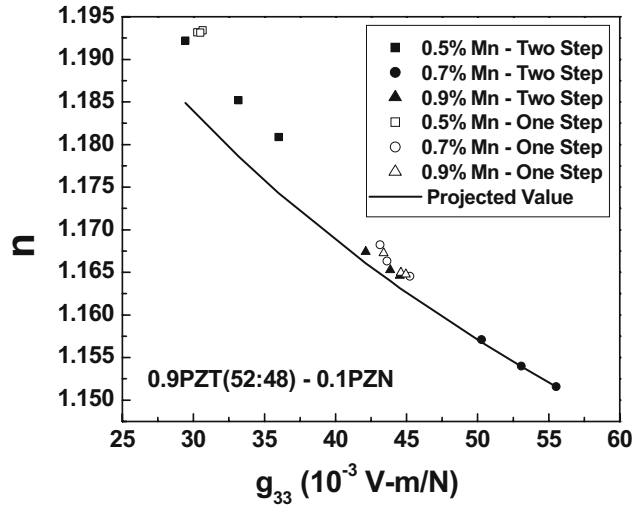

Fig. 9 Variation of material constant, n, as a function of piezoelectric voltage coefficient, g_{33} for 0.9PZT (52: 48)−0.1 PZN + y wt.% $MnCO_3$

where d is the piezoelectric strain constant and g is the piezoelectric voltage constant. Equation 15 shows that for a given material of fixed area and thickness, a material with high (d.g) product and high g constant $\left(=\frac{d}{\varepsilon\varepsilon_0}\right)$ will generate high voltage and power when the piezoelectric ceramic is directly employed for energy harvesting and sensing. In general, the variation in the magnitude of piezoelectric stress constant and dielectric constant is similar and they increase or decrease simultaneously upon modification with dopants or processing technique resulting in minor changes in the magnitude of g constant.

Recently, the condition for obtaining large magnitude of d.g was derived to be as [31, 32]:

$$|d| = \varepsilon^n \tag{16}$$

where ε is permittivity of the material and n is a material constant having lower limit of 0.5. Using Eq. 14 the maximum magnitude of the product (d.g) can be shown to be given as:

$$\text{Max(d.g)} = \varepsilon^{2n-1} \tag{17}$$

It was found that for all practical polycrystalline piezoelectric ceramic materials the magnitude of n lies in the range of 1.1–1.30. For example—APC 841 (APC International, Mackeyville, PA) with $d_{33} = 300 \times 10^{-12}\ C/N$ and relative dielectric constant $\varepsilon_{33}/\varepsilon_o = 1,350$ represents the conventional hard ceramic. Substituting these values in Eq. 16 it can be shown that the magnitude of n is of the order of ~1.202. Similarly for a conventional soft ceramic such as APC 856 with $d_{33} = 620 \times 10^{-12}\ C/NN$ and relative dielectric constant $\varepsilon_{33}/\varepsilon_o = 4,100$ the magnitude of n is of the order of ~1.237. As the magnitude of n decreases towards unity a giant enhancement in the magnitude of g is obtained. This can be easily seen for the three extreme cases: quartz single crystal (d_{33}=2.3 pC/N, $\varepsilon_{33}/\varepsilon_o = 5$, g_{33}=51.9, n=1.124) (http://www.americanpiezo.com), PVDF piezoelectric polymer (d_{33}=33 pC/N, $\varepsilon_{33}/\varepsilon_o = 13$, g_{33}=286.7, n=1.054) [33], and relaxor piezoelectric single crystals such as PZN −7%PT (d_{33}=2,500 pC/N, $\varepsilon_{33}/\varepsilon_o = 6,700$, g_{33}=42.1, n=1.190) [34]. Thus to obtain a large magnitude of the product (d.g), the piezoelectric compositions can be tailored by modifying with the dopant or processing technique such that the change in piezoelectric and dielectric constant leads to a decrement in the magnitude of constant n.

We have optimized the magnitude of the (d.g) in the system given as $0.9Pb(Zr_{0.52}Ti_{0.48})O_3-0.1Pb(Zn_{1/3}Nb_{2/3})O_3$+0.5, 0.7 and 0.9 wt.% $MnCO_3$. The ceramics were synthesized using the conventional mixed oxide sintering. Two types of sintering profiles were used—one step (conventional, 1,050 °C for 2 h) and two step. In two step sintering the samples were kept at 1,050 °C for 5 min and then temperature was dropped to 950 °C and held for 4 h. A heating rate of 3 °C/min and cooling rate of 7 °C/min was used [32]. It has been shown that one step sintering is not suitable for producing small grain sizes because the final stage of sintering process is always accompanied by rapid grain growth [35]. The capillary driving force for sintering and grain growth produces very large grain in one step sintering. A simple two step sintering suppress the final stage grain growth and small grain sizes are achieved by controlling the kinetics of grain boundary diffusion and grain boundary migration [35]. The logarithmic relationship between the constant n and g was found to be obeyed by all the synthesized samples as shown in Fig. 9 [32]. Figure 10 compares the composition given by $0.9\ Pb(Zr_{0.52}Ti_{0.48})O_3-0.1\ Pb(Zn_{1/3}Nb_{2/3})O_3$+0.7 wt.% $MnCO_3$ denoted as UTA (n=1.151) with the data available for the commercial compositions.[1] Assuming the magnitude of applied stress equal to 1/6th of the compressive strength for the piezoelectric ceramic (~100 MPa) than the energy density computed using Eq. 15 for the composition UTA is found to be 80.84 mJ/cm^3.

[1] Data for commercial polycrystalline piezoelectric ceramic compositions: *EDO Corporation* (EC-98: $d_{33}.g_{33}$=11,388×10^{-15} m^2/N, g_{33}=15.6× 10^{-3} m^2/C, and n=1.249); *EDO Corporation* (EC-65: $d_{33}.g_{33}$=9,500×10^{-15} m^2/N, g_{33}=25×10^{-3} m^2/C, and n=1.205); *Fuji Ceramics Corporation* (C-8 : $d_{33}.g_{33}$=12,351×10^{-15} m^2/N, g_{33}=19.7×10^{-3} m^2/C, and n=1.225); *Morgan Electroceramics* (PZT-507 : $d_{33}.g_{33}$=14,000×10^{-15} m^2/N, g_{33}=20×10^{-3} m^2/C, and n=1.226); *Morgan Electroceramics* (PZT 701 : $d_{33}.g_{33}$=6,273×10^{-15} m^2/N, g_{33}=41×10^{-3} m^2/C, and n=1.165); *APC International* (APC 855 : $d_{33}.g_{33}$=12,600×10^{-15} m^2/N, g_{33}=21×10^{-3} m^2/C, and n=1.223); *APC International* (APC 850 : $d_{33}.g_{33}$=10,400×10^{-15} m^2/N, g_{33}=26×10^{-3} m^2/C, and n=1.203); *Channel Industries* (5600 Navy: $d_{33}.g_{33}$=11,110×10^{-15} m^2/N, g_{33}=22×10^{-3} m^2/C, and n=1.217); *Channel Industries* (5400 Navy: $d_{33}.g_{33}$=7,830×10^{-15} m^2/N, g_{33}=26.1×10^{-3} m^2/C, and n=1.199); *Ferroperm* (Pz24: $d_{33}.g_{33}$=10,260×10^{-15} m^2/N, g_{33}=54×10^{-3} m^2/C, and n=1.150); *DongIl* (D211: $d_{33}.g_{33}$=8,820×10^{-15} m^2/N, g_{33}=42×10^{-3} m^2/C, and n=1.166).

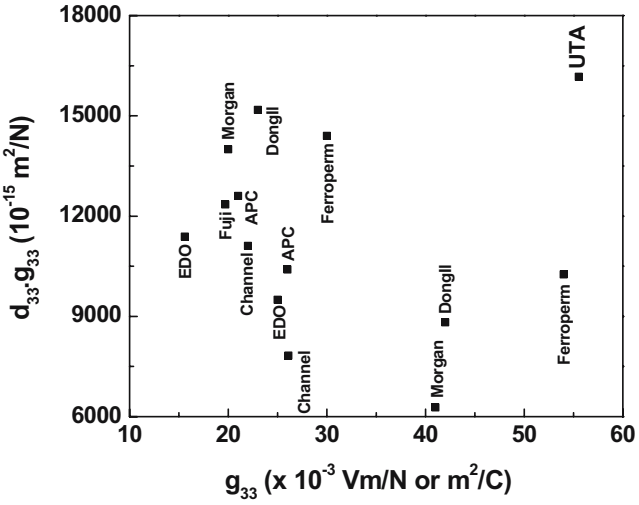

Fig. 10 Comparison of the magnitude of product ($d_{33}.g_{33}$) as a function of g_{33} for the material developed in this study with commercially available ceramics. The material denoted as UTA represents 0.9 $Pb(Zr_{0.52}Ti_{0.48})O_3-0.1Pb(Zn_{1/3}Nb_{2/3})O_3+0.7$ wt.% Mn and has the properties $d_{33}.g_{33}=16{,}168\times10^{-15}$ m^2/N, $g_{33}=55.56\times10^{-3}$ m^2/C, and $n=1.151$. The data for other compositions are listed in [36]

5 Piezoelectric material selection in on-resonance condition

Energy harvesting in the on-resonance condition is limited due to limitation in terms of vibration amplitude at high frequencies. The material requirements for the energy harvesting device operating under high frequency resonance condition are similar to that required for the piezoelectric transformer. A piezoelectric transformer converts the electrical energy into mechanical energy at the input terminal and mechanical to electrical energy at the output terminal. The three most critical parameters for the selection of the piezoelectric material operating under mechanical resonance are mechanical quality factor, electromechanical coupling factor, and dielectric constant and a high magnitude for all these parameters is desired. This is because of the fact that in each electromechanical transformation, the energy of the system reduces by a factor of k^2, and a material with higher capacitance will have lower impedance and hence it can draw higher current. From materials point of view, above requirements translate into designing a material, which has combinatory characteristics of conventional hard

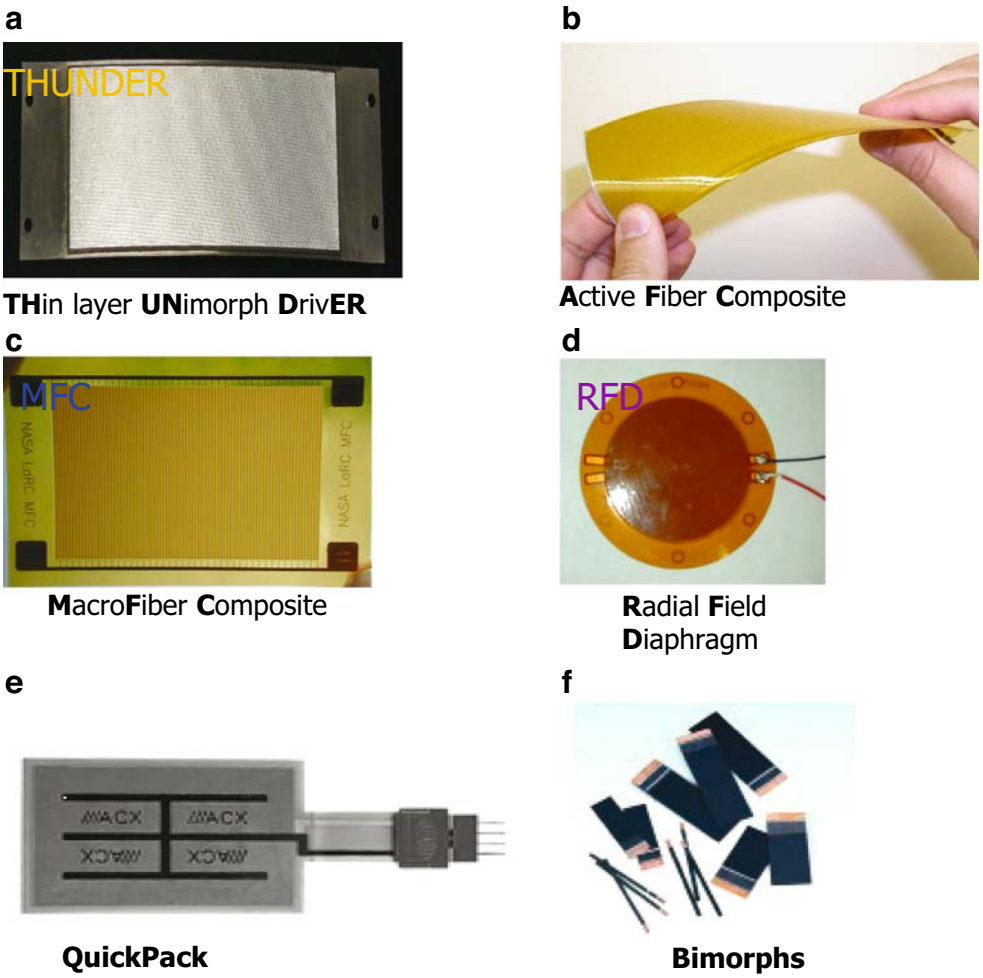

Fig. 11 List of the low profile piezoelectric transducers. **a** Thunder, **b** Active Fiber Composite, **c** Macro Fiber Composite, **d** Radial Field Diaphragm, **e** QuickPack, and **f** Bimorp

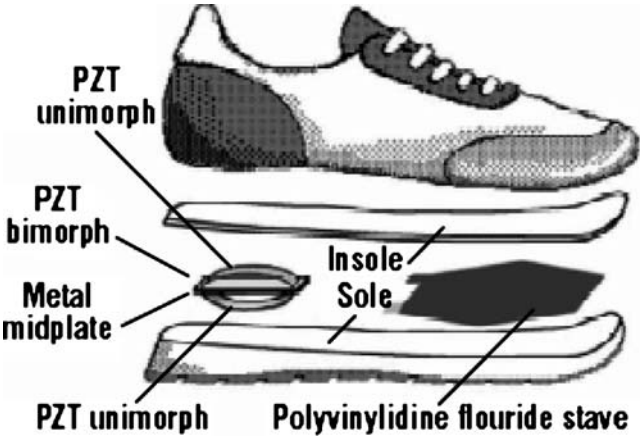

Fig. 12 Integration of a flexible PZT Thunder clamshell and a 16-layer polyvinylidine flouride bimorph stave under the insole of a running shoe [12] (Source: http://www.media.mit.edu/resenv/power.html)

and soft material. Generally, PZT is modified with a complex A or B-site ion (Pb based relaxor type materials) in various ratios and some acceptor ion is added to this composition. Adding the relaxor type compounds enhances the piezoelectric properties of the material while the acceptor ion increases the mechanical quality factor and reduces dielectric losses.

6 Energy harvesting using low profile piezoelectric transducers

Low profile transducers are attractive for piezoelectric harvesting applications for several reasons including, light weight, flexibility, easy mounting, large response, and low frequency operation (the terminology low-profile has been used to describe the transducer structure which posses all these qualities). Figure 11 shows the list of the promising low profile transducers in energy harvesting applications. All these transducers are commercial products and widely available.[2] Pre-stressed transducers such as Thunder consist of a sandwich structure where the bottom layer is stainless steel, the middle layer PZT ceramic, and the top layer is aluminum. LaRC™-SI is used as the adhesive between the layers. During the cooling of the whole structure from high temperature (~300 °C), the mismatch in coefficients of thermal expansion causes the metal and ceramic layers to contract at different rates, imparting a characteristic bend and leaving the ceramic in pre-stress condition as shown in Fig. 11a. Thunder elements have been used to harvest the energy from the walking motion with a net transfer of 2 mJ per step as shown in Fig. 12. Another transducer has been developed on the similar principle by Konkuk University called as Lipca, where the metallic layers have been substituted with fiberglass and unidirectional carbon. Experimental results have demonstrated that Lipca provides higher displacement than the Thunder however; the performance is not as consistent [36]. Further, Lipca is lighter than Thunder making it suitable for tapping vibrations.

Piezoelectric active fiber composites (AFC's) developed by Advanced Cerametrics, Inc (ACI) have been demonstrated in harvesting the electrical energy from the heel strike.[3] The transducer consists of uniaxially aligned piezoelectric fibers surrounded by polymer matrix and can include inactive glass fibers for enhanced strength as shown in Fig. 11b. Interdigital electrodes are used to apply the electric along the length of the fiber. The piezoelectric fibers are synthesized using the technology called Viscose Suspension Spinning Process (VSSP) and are typically circular in cross-section. Figure 13 shows the picture of the fabricated fiber and the sintered microstructure. The experiment consisted of dropping the steel ball on multilayer composite and measuring the output voltage. The ball weight was 33 g and the drop distance was 10 cm [37]. Figure 14 illustrates the effect of the transducer thickness on the output voltage for various fiber diameters. The maximum voltage of 350 V (DC) was found for the 5.85 mm thick transducer made using 15 μm diameter fiber. The peak power in this case was measured to be 120 mW for 0.3 ms [38].

Macro fiber composite (MFC), shown in Fig. 11c, was developed at the NASA Langley Research Center also has uniaxially aligned fibers surrounded by a polymer matrix similar to AFC's, however the fibers have a rectangular cross-section. MFCs are marketed by Smart Materials Corporation, FL [39]. The fibers in MFCs are machined from low-cost piezoelectric ceramic wafers using a computer controlled dicing saw. MFC's can be operated in either d_{33}-mode or d_{31}-mode by designing the two different electrode patterns as shown in Fig. 15. MFC operating in d_{33}-mode has higher energy conversion rate but lower electrical current as compared to that d_{31}-mode as shown in Table 6 [40]. These transducers have been shown to have the reliability of over 10^9 cycles operating at maximum strain. The energy harvesting tests conducted on the two kinds of MFC's has shown that:

(1) d_{33} effect MFC less suitable for energy harvesting due to high voltage and lower charge output
(2) Electric charge generated is proportional to strain frequency, and
(3) Low strain, high frequency (>20 Hz) is suitable for continuous charge generation

[2] Thunder—Face International Corp., Norfolk, VA. ; AFC—Advanced Cerametrics Inc., Lambertville, NJ; MFC—Smart Materials Corp., Sarasota, FL; RFD—NASA Langley Research Center, Hampton, VA; QuickPack—Mide Technology, Medford, MA; Bimorphs—APC International, Mackeyville, PA.

[3] See footnote 2.

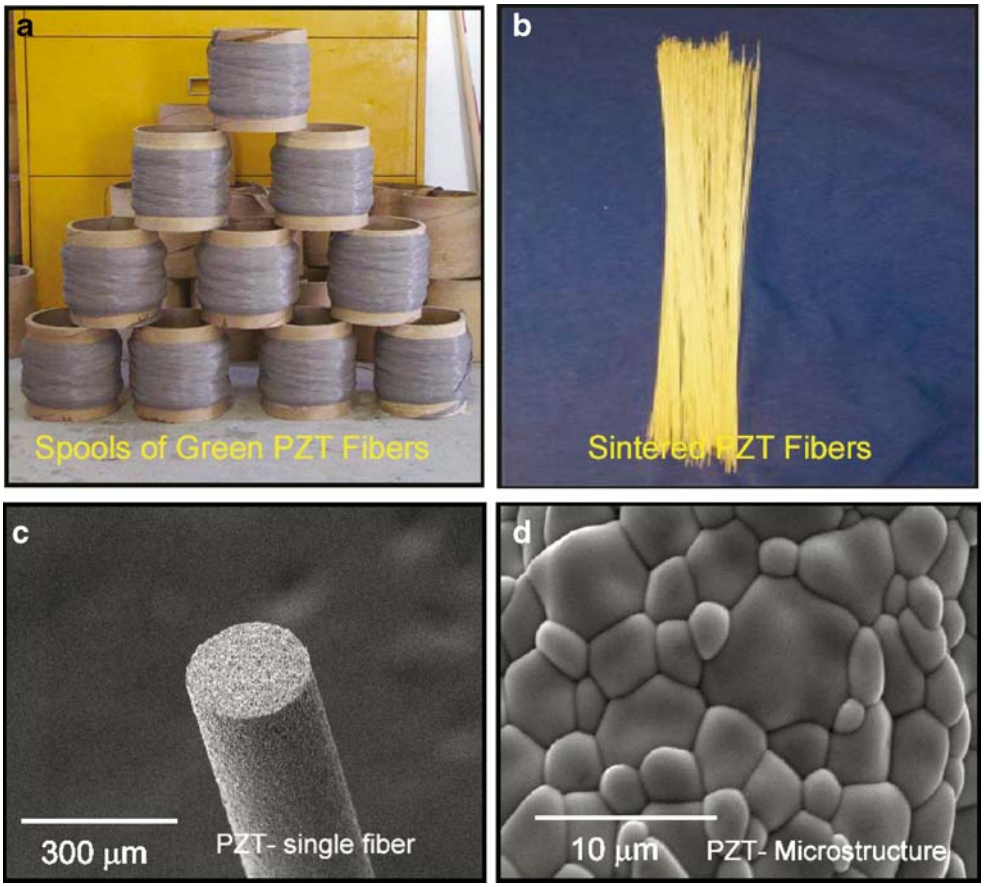

Fig. 13 Fiber produced by the ACI. **a** Spools of fibers produced by the Viscose Suspension Spinning Process (VSSP), **b** Sintered fibers, **c** Microstructure of the single fiber showing circular cross-section, and **d** grain structure exhibiting high density (Source: Advanced Cerametrics Inc. website, http://www.advancedcerametrics.com/. Permission granted by ACI to reproduce the figure)

Smart Materials Corp. have recently revealed a micro-energy harvester TI MSP430 μController based on MFC's which is integrated with EnOcean STM100 and has the ability to measure the local temperature, pressure and other environmental variables [40]. The picture of the prototype is shown in Fig. 16a. MicroStrain has also developed a wireless sensor node using the MFC's as shown in Fig. 16b which has been demonstrated to operate with one of the highest efficiencies [41].

NASA LaRC's Radial Field Diaphragm (RFD) is an exciting development in the area of low profile piezoelectric transducers. The RFD comprises of a thin circular piezoelectric ceramic disk sandwiched between two polyimide dielectric films with copper-etched spiral electrodes as shown in Fig. 11d [42]. On each spiraled electrode pattern, positive and negative electrodes spiral inward to the center of the disk in a serpentine manner. This novel electrode pattern induces an electric field into the piezoelectric ceramic that extends out radially from the center of the wafer. The dielectric film serves as the electrode carrier and insulator. At low frequencies of DC—10 Hz, RFD's have been shown to provide 2–3 times higher displacement as compared to conventional unimorphs [42]. Experimental demonstration of the RFD's in the energy harvesting application has not yet been reported.

QuickPack (rigid) and PowerAct (flexible) transducer are packaged bimorphs in a protective skin with pre-attached electrical leads, producing a highly reliable component with no soldered wires (http://www.mide.com). These transducers have been demonstrated in energy harvesting applications by exciting them with a mechanical shaker at resonance frequency and measuring the response. QuickPack model QP20W having dimensions of 5.08× 3.81×0.051 cm^3 with a nominal capacitance of 200 nF

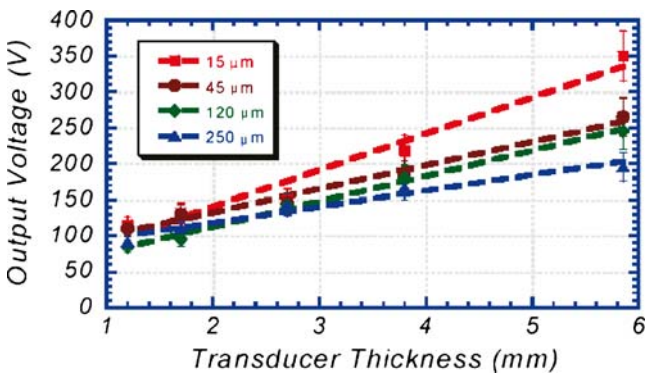

Fig. 14 Variation of the output voltage as a function of the fiber composite thickness for various fiber diameters (Source: Advanced Cerametrics Inc. website, http://www.advancedcerametrics.com/. Permission granted by ACI to reproduce the figures)

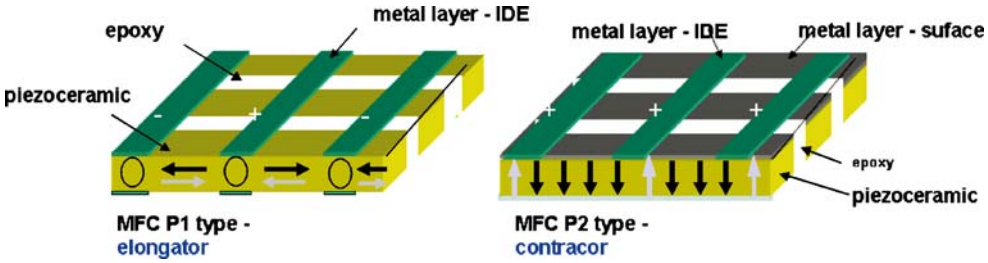

Fig. 15 Illustration of the two different types of MFCs (1) d_{33}-mode and (2) d_{31}-mode. (Source: Technical paper presented by Smart Material Corp. at UTA Workshop 2006. Permission granted by T. Daue to reproduce the figure.)

driven at 50 Hz has been shown to provide 30.66 mW power with the open circuit voltage of 68 V [15, 43].

In general, piezoelectric bimorph transducer is the simplest and well known low frequency resonance structure. Bimorphs can be easily mounted into several configurations as shown in Fig. 17 providing high degree of adaptability to the available vibrations. Recently, we have demonstrated wind energy harvesting using the bimorph transducer commercially available from APC International, Mackeyville, PA (http://www.americanpiezo.com). Bimorph transducer has following advantages in terms of suitability for windmill:

1. They have enough mechanical strength in the vibration frequency range of 1–10 Hz. In this range the applied load on the bimorph can be of the order of few Newton's. Laboratory scale measurements have shown that a bimorph vibrating under a force of 2 N at low frequencies of 10 Hz do not suffer from any mechanical degradation.
2. The piezoelectric voltage coefficient of bimorph is high so the charge developed under fully loaded condition is high.
3. The maximum displacement of the bimorph is significant due to the high level of bending force that can be applied.
4. The manufacturing cost of bimorph is very low.

Compared to mechanical vibrations from automobile, walking, rotary machines and water flow, wind is far more attractive source of electrical energy. It is available everywhere making the technology to be implemental on a universal platform. *The wind is a by-product of solar energy.* As long as there is sunlight, there will be wind. The surface of the earth heats and cools unevenly, creating atmospheric pressure zones that make air flow from high- to low-pressure areas. Approximately 2% of the sun's energy reaching the earth is converted into wind energy. For a flow of air with velocity ν and density ρ through unit area A perpendicular to the wind direction, the kinetic energy per unit time is given by P (http://www.Windworkers.com; http://www.windturbinewarehouse.com; http://www.windpowerstore.com) [44]:

$$P = {}^1\!/_2 m v^2 = {}^1\!/_2 (A v \rho) v^2 = 1/2 A \rho v^3 \tag{18}$$

The air density varies with altitude, atmospheric pressure and temperature. The power density function $p(\nu)$ of a windmill may be expressed as (http://www.Windworkers.com; http://www.windturbinewarehouse.com; http://www.windpowerstore.com):

$$p(\nu) = C_p {}^1\!/_2 A_r \rho \nu^3 f(\nu) \quad \text{and}$$
$$f(\nu) = \left({}^k\!/_c\right)\left({}^\nu\!/_c\right)^{k-1} e^{-\left({}^\nu\!/_c\right)^k} \tag{19}$$

where C_p is the power coefficient of the windmill defined as the ratio of the power output from the windmill to energy available in the wind, $f(\nu)$ is the wind speed probability density function, A_r is the rotor area, k is the shape parameter and c is the scale parameter. The coefficient C_p is limited to 0.59 by the Betz limit. Windmills are generally designed such that maximum efficiency occurs at wind velocities around 8 m/s (or about 18 mph). Efficiency is dependent on wind velocity, and average operating efficiencies are usually about 20%. At low air velocity, efficiency can be lower than 20%. Wind power density is a term commonly used to describe the wind power available per unit area swept by the blades. Roughly, wind power density

Table 6 Comparison of the sensor and actuator characteristics for the d_{33} and d_{31} mode MFCs (Permission granted by T. Daue, Smart Materials Corp to reproduce the figure).

Device	Operation voltage		Capacity	Sensor Characteristic		Actuator characteristic	Generator characteristic
	$V_{op}^{+}[V]$	$V_{op}^{-}[V]$	C_{pol} [nF/cm^2]	$d_{31}^{eff}[pC/N]$	$d_{31}^{eff}[pC/N]$	Strain/Volt. [μstrain/V]	Charge/Strain[pC/ppm]
3–3 MFC	1,500	−500	0,42	460	–	0,7..0,9[0 ... 1,500 V]	1,670 [>100 V]
3–1 MFC	360	−60	4,5	–	−370	−2 [0 ... 360 V]	3,250 [<100 V]

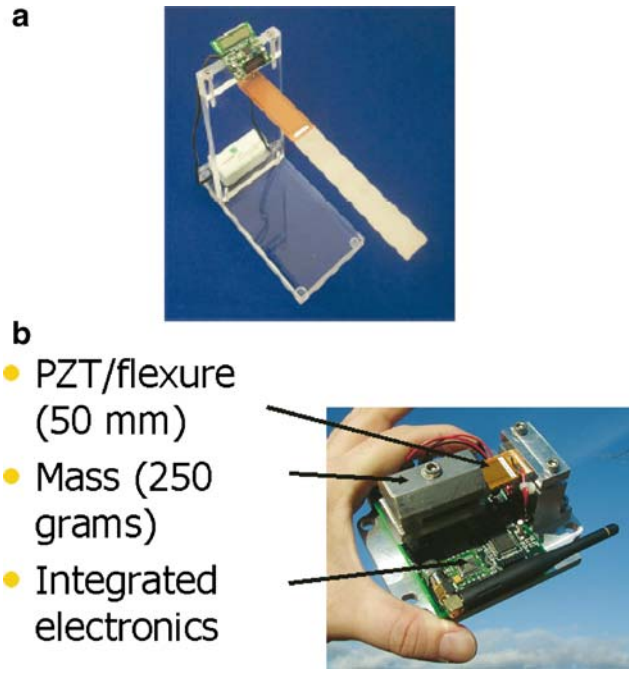

Fig. 16 Prototype devices developed using the MFC's. **a** Wireless Temperature/Pressure sensor from Smart Materials Corp./EnOcean (Source: Technical paper presented by Smart Material Corp. at UTA Workshop 2006. Permission granted by T. Daue to reproduce the figure), and **b** Wireless sensor node from MicroStrain (Source: Technical paper presented by MicroStrain at UTA Workshop 2006 Permission granted by S. Arms to reproduce the figure)

$=0.056\ \nu^3$ where ν is in miles per hour. It can be seen from this expression that a large amount of power is available even with nominal wind velocities and efficiencies of the 10–20%.

The structure and frame-work of the piezoelectric windmill is similar to that of conventional windmill except it has active piezoelectric blades [45, 46]. As the wind flows through the windmill the active blades oscillate in turn producing electricity. Figure 18 shows the schematic of the piezoelectric windmill which consist of 10 bimorph transducers arranged along the circumference. The dimensions of each individual bimorph were $60\times20\times0.6\ mm^3$ with a free length of 53 mm [45]. The resonance frequency and capacitance for this size of bimorph was measured to be 65 Hz and 170 nF, respectively. The arrangement of the transducers is made such that corresponding to wind flow the piezoelectric transducer oscillates between the stoppers. The oscillatory motion is generated using the cam-shaft gear mechanism. The continuous back and forth oscillation of bimorph between the two stoppers will continuously generate electricity. The characterization of the windmill was done inside a long square tube. Wind was blown in the tube using a fan. Wind speed was measured using EA-3010U anemometer fitted at the top of the mill. The voltage was monitored on the HP 54601A digital 4-channel oscilloscope using HP 10071A probe. A full-bridge rectifier circuit using the low power diodes was fabricated and the voltage was measured across a capacitor. Figure 19 shows the power-speed relationship for the fabricated windmill. The cut-in wind speed (threshold wind speed required to start the windmill) was found to be 4.7 mph and cut-out wind speed (maximum wind speed above which operating could result in harm to the structure) was found to be 12 mph. The rated wind speed was found to be 10 mph providing a constant power of 7.5 mW. The solid line shown in this figure is just for the guide to the eyes [19].

Kim et al. have demonstrated the capability of harvesting the electrical energy from mechanical vibrations in a dynamic environment through a "Cymbal" piezoelectric transducer [47, 48]. The mechanical vibrations were in the range of 50~150 Hz with force amplitude of the order of 10 N. The metal cap enhances the endurance of the ceramic to sustain high loads along with stress amplification. The experiments were performed at a frequency of 100 Hz on a cymbal with a 29 mm diameter and a 1 mm thickness under force of 7.8 N. At this frequency and force level, a power of 39 mW was generated from the cymbal, which was measured across a 400 kΩ resistor. This magnitude of power from one cymbal is quite impressive however the force and frequency level are also quite high.

In spite of these developments there are several challenges remaining in the implementation of the low profile piezoelectric energy harvesting system including (1) power density (power per unit volume of total device structure), (2) reliability (maximum number of cycles before mechanical or electrical breakdown), and (3) cost-effectiveness (total dollar cost for fabrication and installation of the system). The major factor which hinders the implementation of energy harvesting devices in practical applications is higher cost as compared to that of batteries. As the research in this area continues it will be important to realize scenarios where the high cost of energy harvesting devices could be overlooked.

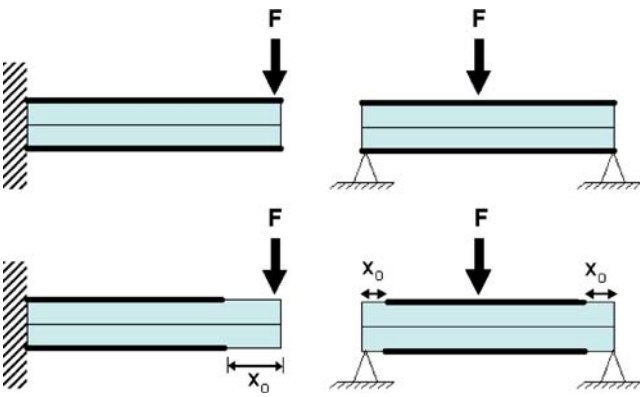

Fig. 17 Schematic representation of the various ways of loading the bimorph transducers

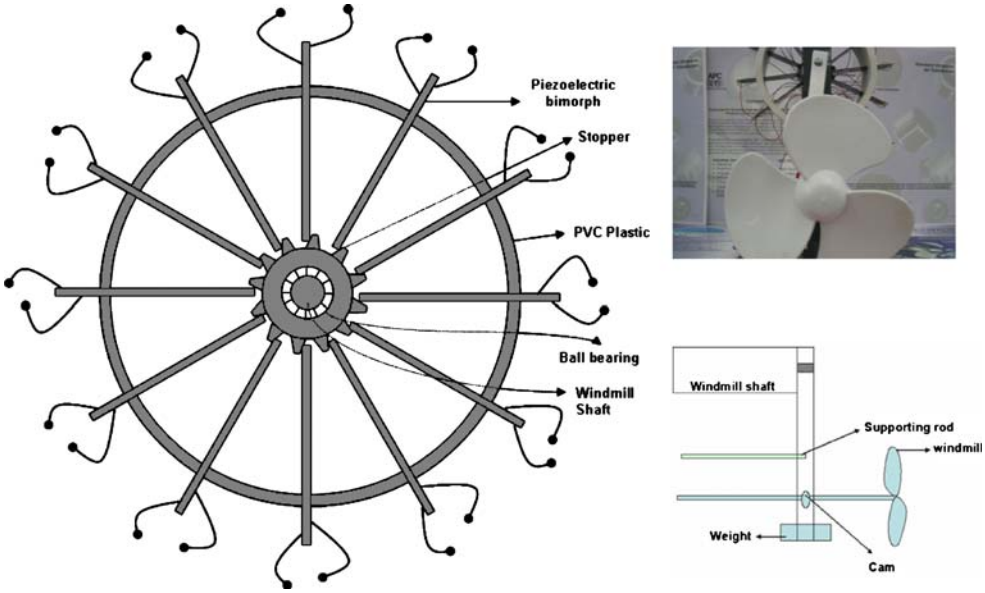

Fig. 18 Schematic diagram of the piezoelectric windmill showing the arrangement of piezoelectric actuators

7 Energy harvesting using piezoelectric polymers

Researchers from Ocean Power Technologies have proposed energy harvesting Eel that uses piezoelectric polymer to convert the mechanical flow energy available in oceans and rivers to electrical power [49]. In a nonturbulent flow, the bluff body regularly sheds alternating vortices on either side of the bluff body with a frequency and size corresponding to the flow speed and width of the bluff body. The resulting pressure differential caused by the vortices forces the Eel to move in an oscillating motion. The resulting strain on the piezoelectric polymer generates a low frequency ac voltage signal. The electrical power, P, produced by an Eel undulating in water flow is given by [49]:

$$P = \frac{\eta_1 \eta_2 \eta_3 A \rho V^3}{2} \tag{20}$$

where η_1, η_2, η_3 are hydrodynamic, piezoelectric and circuit efficiencies, A is the cross-sectional area of the Eel, ρ is the density of the water, and V is the velocity of the water flow. Initially, PVDF was chosen as the piezoelectric material.

PVDF is a semi-crystalline high-molecular weight polymer with repeat unit (CH2–CF2) whose structure is essentially head-to-tail, i.e., CH2–CF2–(CH2–CF2)*n*–CH2–CF2. PVDF is approximately half crystalline and half amorphous. In semicrystalline polymers such as PVDF, there are regions where the chains exhibit a short and long term ordering (crystalline regions). A net dipole moment (polar phase) is obtained by applying a strong electric field at or above T_g and then is frozen in by cooling the material resulting in a piezoelectric-like effect. The curie temperature of PVDF is near 110 °C which makes it useful for some elevated temperature operations [50–54]. Our investigations have shown that the piezoelectric properties maintain high magnitude until 70 °C. Deposition of PVDF films is now a well established technique [51, 54]. In the sol-gel process, PVDF powder is dissolved in a solvent composed of 90% acetone and 10% dimethylformamide (DMF) and sonicated in an ultrasonic water bath. The solution is applied on the substrate through spin coating at room temperature, followed by drying at room temperature or in an oven.

Sohn et al. have investigated the feasibility of using PVDF films of thickness 9–110 μm for powering the Bio-MEMS using the FE analysis package MSC/NASTRAN

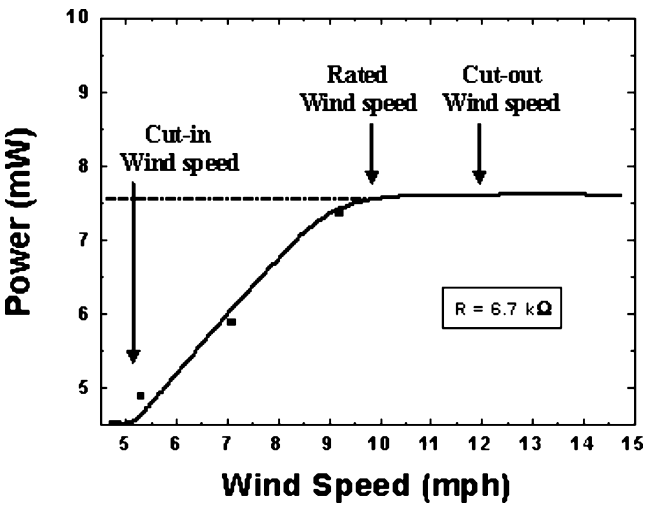

Fig. 19 Power-Speed relationship for the fabricated piezoelectric windmill. The typical parameters of the windmill were found to be cut-in speed=4.7 mph, cut-out speed=12 mph, rated wind speed=10 mph and rated power=7.5 mW

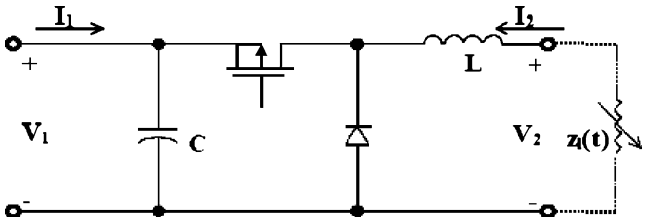

Fig. 20 Switch implementation in the direct down (or buck) converter with load.

[55]. The results showed that square (cross-section—10× 10 mm^2, thickness=28 μm) and circular (radius=5.62 mm, thickness=28 μm) piezo-films when stressed under pressure of 5,333 N/m^2 (or 5.333 mN/mm^2) at 1 Hz frequency produce electrical power levels of 0.25 and 0.33 μW, respectively. This result showed the possibility of utilizing the piezo-films for powering the DNA telecommunications chip implanted in the human body which requires total power of 10 mW [55–57]. Based on the normal blood flow conditions it was found that a time period of 8–10 h will be required for one complete operation.

PVDF has the advantage that it is mechanically strong, is resistant to wide variety of chemicals, including acids and it can be manufactured on a continuous reel basis. However, PVDF has a relatively low value of d_{31} (3.3×10^{-11} pC/N) resulting in lower power. This prompted research on electrostrictive polymers where it is possible to induce large piezoelectric effect by applying high DC bias field due to Maxwell stress. Electrostrictive polymers recently have been discovered that generate large strain (above 5%) under moderate electric field intensity (400–800 V on a 20 μm film) [58]. Poyl(vinylidene fluoride-trifluoroethylene), or P[VDF:TrFe] copolymers have been shown to exhibit d_{31} of 8.0×10^{-11} pC/N, and polyurethane has d_{31} of 1.7×10^{-10} pC/N. A theoretical investigation conducted by Liu et al. has shown that the energy densities of the order of 0.221 J/cm^3 is possible in the constant field condition using polyurethane material [59]. In future it is expected that the piezoelectric and electrostrictive polymers will assume significant importance owing to their flexible nature which allows integration with almost any structure.

8 Energy storage circuit

In the bulk harvester cases, a DC-to-DC converter circuit is commonly used to harvest the generated electric energy and transfer it across the load as schematically shown in Fig. 20 [15, 43, 47, 48]. The impedance for applications such as charging a battery and lighting a bulb is in the order of few hundred ohms while the piezoelectric is a high impedance load. This converter circuit is called a buck converter and it operates in the discontinuous current mode (DCM). The optimal duty cycle of the converter is dependent on inductance, switching frequency, the piezoelectric element's capacitance, and the frequency of mechanical excitation of the piezoelectric device. Figure 21 compares the load line with and without the DC–DC converter [47]. It can be easily seen from this figure that the converter significantly reduces the matching impedance of the circuit and provides a constant load line. The optimal duty cycle of the converter is given as [15]:

$$D_{\text{opt}} = \sqrt{\frac{4\omega L C_{\text{p}} f_s}{\pi}} \tag{21}$$

where ω is the angular frequency of mechanical excitation, L is the inductance, C_{p} is the damped capacitance of piezoelectric element, and f_{s} is the switching frequency.

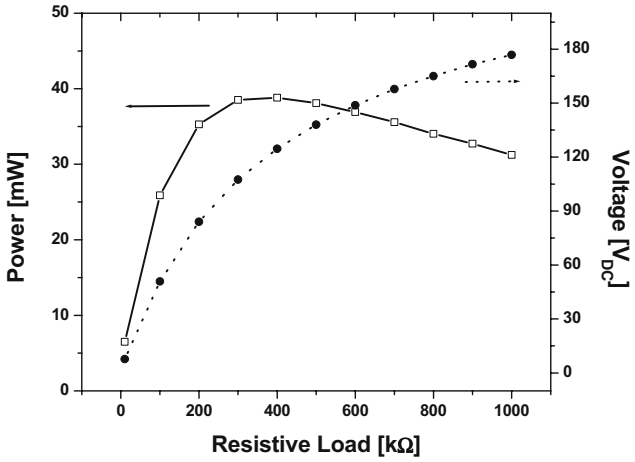

a Without DC-DC converter

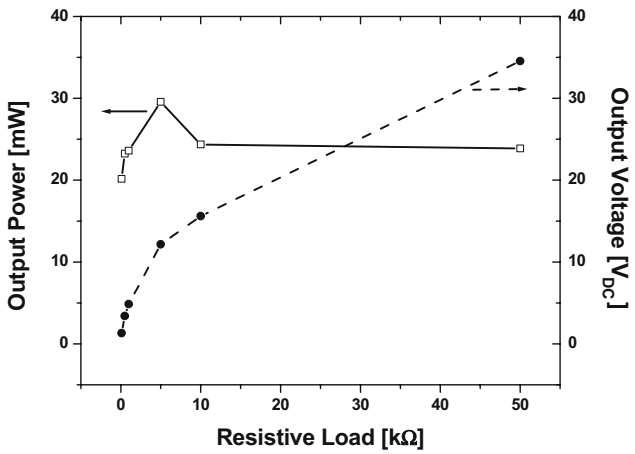

b Output of DC-DC converter

Fig. 21 Output voltage and output power of the DC–DC converter as a function of resistive load condition with 1 kHz switching frequency and 2% duty cycle using single layered high-g PZT Cymbal transducer at 8 N

Several other techniques are used in conjunction with the circuit for reducing the matching impedance to lower levels such as multilayering the piezoelectric transducer structure and increasing the area aspect ratio (area/thickness).

Recently, Guyomar et al. have presented a nonlinear processing technique "Synchronized Switch Harvesting on Inductor" (SSHI) for harvesting energy, which consists of a switching device in parallel with piezoelectric element [60]. This device is composed of a switch and an inductor connected in series. The switch is in open state except when the maximum displacement occurs in the transducer. At that instant the switch is closed and the capacitance of the piezoelectric element and inductance together constitute an oscillator. The switch is kept closed until the voltage on the piezoelectric element has been reversed. In case of nonlinear AC device, a resistive load is directly related on the piezoelectric element in parallel with the switching device. This nonlinear technique has been shown to significantly enhance the performance of the energy harvesting circuit and will be well suited for the resonating structures [60].

9 Energy harvesting using piezoelectric micro devices

Self-powering at chip scale can be achieved by developing a smart architecture which utilizes all the environmental resources available for generating electrical power as shown in Fig. 22 for vibrations, light, and temperature gradients. This architecture has been proposed and analyzed by Priya et al. for the self powered ultra high efficiency sensor network with static and mobile nodes [61]. The power harvested can be stored using switched-capacitor dc–dc converter (regulated charge pump) through on-chip chemical storage media. Regulated charge pump is preferred over the switched-mode power converter (SMPC) and low-dropout regulator (LDR) because (1) SMPC requires inductor for dc–dc conversion; however the inductor to sustain milliampere current is complicated for being integrated on the chip, and (2) LDR can only perform step-down operation. Since the input voltage of the dc–dc converter can be as low as 0.1 V, LDR is not suitable [62]. Amirtharajah and Chandrakasan have reported a test chip fabricated using CMOS process that integrates an ultra-low power controller to regulate the generator voltage and a low power subband filter DSP load circuit [63]. The entire system was found to consume a total of 18 μW power. Several other methodologies have been proposed in literature power conditioning of piezoelectric micro devices [64–69]. These results clearly indicate the possibility of realizing an efficient power harvesting system based on the architecture depicted in Fig. 22. One other challenge which needs to be tackled in order to implement this scheme for powering sensors is design and fabrication of an ASIC since outputs from individual layers have widely different impedance.

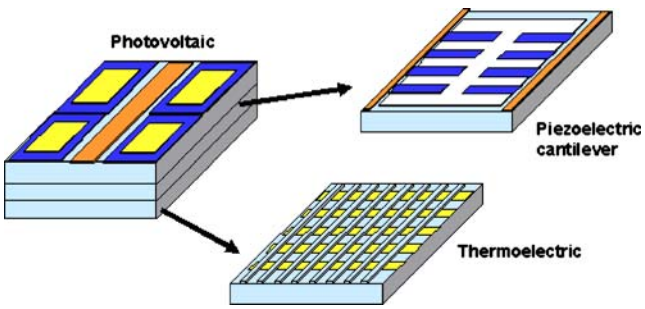

Fig. 22 Schematic representation of the power module harvesting energy from environmental sources light, vibrations and temperature gradients

In this review, a brief description is presented on the middle layer consisting of piezoelectric cantilevers. Lu et al. have analyzed the case of '31' mode piezoelectric micro-cantilever structure and developed a model for power and coupling efficiency (kinetic to electric energy conversion) as a function of frequency [70]. It was found that power increases with frequency while the coupling efficiency decreases. The modeling results also indicated that at low frequencies the output power requires smaller dielectric constant (ε_{33}) while at higher frequencies it's the ratio of piezoelectric constant (e_{31}) and dielectric constant that makes significant contribution. The power generated from the cantilever beam depends on several factors including resonant frequency, end mass, and mechanical damping. The resonant frequency of the free-end beam is approximately given by:

$$f_o = \sqrt{\frac{k}{m}} = \sqrt{\frac{Eh^3w}{4L^3m}} \tag{22}$$

where k is the mechanical spring constant, m is the mass, E is the Young's modulus, h is the height of the beam, w is the width of the beam, and L is the length of the beam. The viscous damping constant for squeeze-film damping of a plate can be approximated by [7]:

$$\varsigma = \frac{KA^2\eta}{x^3} \tag{23}$$

where ζ is the damping constant, K is a constant of the order of 0.4–0.5, A is the area of beam, η is the viscosity, and x is the gap between the beam and substrate. From Eqs. 22 to 23 it can be seen that a large mass and gap (x) is desirable for obtaining high power.

Fang et al. have reported results on the PZT cantilever beam of the size 2,000 μm (length)×500 μm (width)× 12 μm (thickness) with Ni proof mass of size 500× 500 μm^2 fabricated on to $Si/SiO_2/Ti/Pt$ substrate [71]. A

power level of 1.15 μW with 432 mV AC voltage was measured across a 20.4 kΩ load under resonant vibration of about 609 Hz with 1 g acceleration. This is an interesting result since the power magnitude can be enhanced by arraying the cantilevers in parallel with in-phase operation. Jeon et al. developed a d_{33}-mode piezoelectric power generating device consisting of flat cantilever structure with interdigitated electrode pattern and a proof mass at the end. [72] In this experiment it was found that a 170 μm× 260 μm PZT beam generates 1 μW of continuous electrical power to a 5.2 MΩ resistive load at 2.4 V DC corresponding to an energy density of 0.74 mWh/cm^2. The measurements were conducted at the first resonant frequency of 13.9 kHz [72]. Several other micro-machined devices utilizing PZT cantilever and diaphragm structure have been reported in literature [73–75].

Micro-devices are currently the most pursued areas in the power harvesting and this subject will assume increasing importance as the trend towards lab-on-chip system continues.

10 Summary

Piezoelectric converters are prominent choice for mechanical to electric energy conversion because the energy density is three times higher as compared to electrostatic and electromagnetics. The electrical power generated is inversely proportional to the damping ratio which should be minimized through proper selection of the materials and design. The power is proportional to the square of the acceleration and reaches maximum at the resonance frequency. The resonance frequency of the piezoelectric transducer is dependent upon the configuration, size, and loading conditions. The efficiency (η) of the conversion process in resonance condition is dependent upon the coupling coefficient and mechanical quality factor of the piezoelectric. In the off-resonance condition, the product (d.g) is directly related to the energy density. Recently, the condition for obtaining large magnitude of d.g was derived to be as [29, 30]:

$$|d| = \varepsilon^n$$

where ε is permittivity of the material and n is a material constant having lower limit of 0.5. Several low profile transducers are available commercially which hold significant promise for the energy harvesting applications. Results demonstrated on the MFCs, AFCs, and bimorphs have shown the possibility of realizing a self powered sensor node. In parallel to materials and transducer development, researchers have also developed advanced energy storage circuits. Recent results on circuits utilizing nonlinear signal processing indicate the efficiencies can reach to the theoretical maximum.

As the progress in the development of the power harvesting continues it will be important to standardize the characterization methods so that a comparative study between the systems could be realized.

Acknowledgement The author is grateful for the support from Texas ARP grant 003656-0010-2006.

References

1. J.L. Gonzalez, A. Rubio, F. Moll, Int. J. Soc. Mater. Eng. Resour. **10**(1), 34–40 (2002)
2. J.M. Rabaey, M.J. Ammer, J.L. da Silva, D. Patel, S. Roundy, IEEE Computer **33**, 42 (2000)
3. B. Gates, *The Economist, Special Issue: The World in 2003*, December, 99 (2002)
4. Hitachi, Hitachi unveils smallest RFID chip, RFID Journal, March 14, (2003)
5. T. Douseki, et al., in *ISSCC Digest of Technical Papers*, 84 (1996)
6. T. Ieki, et al., in *Proceedings of IEICE*, September, 39 (1996)
7. S. Roundy, P.K. Wright, J.M. Rabaey, *Energy Scavenging for Wireless Sensor Networks* (Kluwer, Boston, 2004)
8. E.H. Calaway Jr., *Wireless Sensor Networks* (Auerbach, NY, 2004)
9. S. Roundy, E.S. Leland, J. Baker, E. Carleton, E. Reilly, E. Lai, B. Otis, J.M. Rabaey, P.K. Wright, V. Sundararajan, Improving power output for vibration-based energy scavengers, Pervasive Computing, January–March, 28–36 (2005)
10. V. Raghunathan, A. Kansal, J. Hsu, J. Friedman, M.B. Srivastava, in *IEEE International Symposium on Information Processing in Sensor Networks (IPSN)*, April 2005. (TR-UCLA-NESL-200503-10)
11. M. Rahimi, H. Shah, G.S. Sukhatme, in *Proceedings of IEEE International Conference on Robotics and Automation*, Taipei, Taiwan, 14–19 Sept. 2003, pp. 19–24
12. J. Paradiso, T. Starner, Energy scavenging for mobile and wireless electronics, Pervasive Computing, January–March, 18–27 (2005)
13. S. Roundy, P.K. Wright, J. Rabaey, Comput. Commun. **26**(11), 1131–1144 (2003)
14. T. Starner, J.A. Paradiso, in *Low-power Electronics Design*, ed. by C. Piguet (CRC, 2004), Chapter 45, pp. 1–35
15. G.K. Ottman, H.F. Hofmann, A.C. Bhatt, G.A. Lesieture, IEEE Trans. Power Electron. **17**(5), 669–676 (2002)
16. C.B. Williams, R.B. Yates, in *The 8th International Conference on Solid-state Sensors and Actuators, and Eurosensors IX*, Stockholm, Sweden, 25–29 June (1995) pp. 369–372
17. C.B. Williams, C. Sherwood, M.A. Harradine, P.H. Mellor, T.S. Birch, R.B. Yates, IEE Proc., Circ. Devices Syst. **148**(6) 337–342 (2001)
18. H.W. Kim, Ph.D. dissertation, The Pennsylvania State University, University Park, PA, 2006
19. S. Priya, Appl. Phys. Lett. **87** 184101 (2005)
20. K. Uchino, *Ferroelectric Devices* (Marcel Dekker, New York, 2000), p. 169
21. APC International, Piezoelectric ceramics: principles and applications Mackeyville, ISBN 0-9718744-0-9, PA, USA, (2002)
22. K. Sato, K. Okamoto, Y. Fuda, T. Yoshida, Jpn. J. Appl. Phys. **33**, 5378–5380 (1994)
23. M. Umeda, K. Nakamura, S. Ueha, Jpn. J. Appl. Phys. **35**(5B) 3267–3273 (1996)
24. M. Umeda, K. Nakamura, S. Ueha, Jpn. J. Appl. Phys. **36**(5B) 3146–3151 (1997)
25. H.A. Sodano, D.J. Inman, G. Park, Shock Vibr. Dig. **36**(3), 197–205 (2004)
26. H.A. Sodano, G. Park, D.J. Inman, Strain **40**, 49–58 (2004)
27. M. Goldfarb, L.D. Jones, Trans. ASME, J. Dyn. Syst. Meas. Control **121** 566–571 (1999)

28. T. Funasaka, M. Furuhata, Y. Hashimoto, K. Nakamura, Proc. IEEE Ultrasonics Symposium **1**, 959–962 (1998)
29. C.D. Richards, M.J. Anderson, D.F. Bahr, R.F. Richards, J. Micromechanics Microengineering **14**, 717–721 (2004)
30. F. Yamauchi, M. Takahashi, J. Phys. Soc. Jpn. **28**(Suppl.) 313 (1970)
31. R. Islam, S. Priya, Appl. Phys. Lett. **88**, 032903 (2006)
32. R. Islam, S. Priya, J. Am. Ceram. Soc. **89**(10), 3147–3156 (2006)
33. T.T. Wang, J.M. Herbert, A.M. Glass (ed.), *The Applications of Ferroelectric Polymers* (Chapman and Hall, NY, 1988)
34. From the catalog of Microfine Materials Technologies Ltd. available at http://www.microfine-piezo.com
35. I.W. Chen, X.H. Wang, Nature **404**, 168 (2002)
36. K. Mossi, Z. Ounaies, B. Ball, Smith, in *Proceedings of the SPIE, Smart Structures and Materials*, San Diego, CA, vol. 5053, (2003) pp. 423–435
37. S. Leschin, R.B. Cass, F. Mohammadi, in *UTA Workshop on Energy Harvesting*, 27 January 2006
38. Application notes: http://www.advancedcerametrics.com
39. Application notes: http://www.smart-material.com
40. T. Daue, in *UTA Workshop on Energy Harvesting*, 27 January (2006)
41. S.W. Arms, C.P. Townsend, D.L. Churchill, J.H. Galbreath, S.W. Mundell, in *UTA Workshop on Energy Harvesting*, 27 January (2006)
42. R.G. Bryant, R.T. Effinger IV, I. Aranda Jr., B.M. Copeland Jr., E.W. Covington III, in *Proceedings of SPIE, Smart Structures and Materials—Active Materials: Behavior and Mechanics*, Paper 4699-40, San Diego, CA, (2002)
43. G.A. Lesieture, G.K. Ottman, H.F. Hofmann, J. Sound Vib. **269**, 991–1001 (2004)
44. A.G. Davenport, M. Novak, in *Shock and Vibration Handbook*, ed. by C.M. Harris (McGraw-Hill, NY, 1988)
45. S. Priya, C. Chen, D. Fye, J. Zhand, Jpn. J. Appl. Phys. **44**, 104 (2004)
46. C. Chen, R. Islam, S. Priya, IEEE Trans. Ultrason. Ferroelec. Freq. Control **53**(3), 656–661 (2006)
47. H. Kim, A. Batra, S. Priya, K. Uchino, R. E. Newnham, D. Markeley, H.F. Hofmann, Jpn. J. Appl. Phys. **43**(9A) 6178 (2004)
48. H. Kim, S. Priya, K. Uchino, R.E. Newnham, J. Electroceram. **15**, 27–34 (2005)
49. G.W. Taylor, J.R. Burns, S.M. Kammann, W.B. Powers, T.R. Welsh, IEEE J. Oceanic Eng. **26**, 539–547 (2001)
50. Q.X. Chen, D.A. Payne, Meas. Sci. Technol. **6**, 249–267 (1995)
51. C.M. Wang, M.C. Kao, Y.C. Chen, Y.H. Lai, Jpn. J. Appl. Phys. **42**, 170 (2003)
52. H. Kawai, Jpn. J. Appl. Phys. **8**, 975–976 (1969)
53. T.T. Wang, J.M. Herbert, A.M. Glass (ed.), *The Applications of Ferroelectric Polymers* (Chapman and Hall, NY, 1988)
54. M. Benz, W.B. Euler, J. Appl. Polym. Sci. **89**, 1093 (2003)
55. J.W. Sohn, S.B. Choi, D.Y. Lee, Part C: J. Mech. Eng. Sci., 429–436 (2005)
56. J.T. Cain, W.W. Clark, D. Ulinski, M.H. Mickle, Int. J. Parallel Distrib. Syst. Netw. **4**, 140–149 (2001)
57. P. Niu, P. Chapman, R. Riemer, and X. Zhang, in *35th Annual IEE Power Electronics Specialists Conference*, Aachen, Germany (2004)
58. Q.M. Zhang, J. Schienbeim, Electric EAP, in *Electroactive Polymer (EAP) Actuators as Artificial Muscles*, 2nd edn., ed. by Y. Bar-Cohen (SPIE, Bellingham, WA 2004), pp. 95–150
59. Y. Liu, K.L. Ren, H.F. Hofmann, Q. Zhang, IEEE Trans. Ultrason. Ferroelec. Freq. Control. **52**(12), 2411–2417 (2005)
60. D. Guyomar, A. Badel, E. Lefeuvre, C. Richard, IEEE Trans. Ultrason. Ferroelec. Freq. Control **52**(4), 584–595 (2005)
61. S. Priya, D. Popa, F. Lewis, in *2006 ASME International Mechanical Engineering Congress & Exposition*, Chicago, IL, 5–10 November 2006
62. H. Lee, P.K.T. Mok, W.H. Ki, in *Proceedings of IEEE International Symposium on Circuits and Systems*, Geneva, Switzerland, May 2000, vol. I, (2000), pp. 256–259
63. R. Amirtharajah, A.P. Chandrakasan, IEEE J. Solid-State Circuits **33**, 687–695 (1998)
64. B.H. Calhoun, D.C. Daly, N. Verma, D.F. Finchelstein, D.D. Wentzloff, A. Wang, S-H. Cho, A.P. Chandrakasan, IEEE Trans. Comput. **54**, 727–740 (2005)
65. N. Hama, A. Yajima, Y. Yoshida, F. Utsunomiya, J. Kodate, T. Tsukahara, T. Douseki, in *2002 Symposium on VLSI, Circuits Digest of Technical Papers*, Paper 20.2, 280–283 (2002)
66. P.M. Lin, L.O. Chua, IEEE Trans. Circuits Syst. **CAS-24**, 517–530 (1977)
67. J. Siebert, J. Collier, R. Amirtharajah, in *ISLPED'05,* August 9–10 (San Diego, California, 2005), pp. 315–318
68. S. Roundy, P. Wright, J. Rabaey, Comput. Commun. **26**, 1131–1144 (2003)
69. J. Rabaey, A. Chandrakasan, B. Nikolic, *Digital Integrated Circuits: A Design Perspective*, 2nd edn. (Prentice-Hall, Upper Saddle River, NJ, 2003)
70. F. Lu, H.P. Lee, S.P. Lim, Smart Mater. Struct. **13**, 57–63 (2004)
71. H.-B. Fang, J.-Q. Liu, Z.-Y. Xu, L. Dong, D. Chen, B.-C. Cai, Y. Liu, Chin. Phys. Lett. **23**, 732–734 (2006)
72. Y.B. Jeon, R. Sood, J.-H. Jeong, S.-G. Kim, Sens. Actuators A **122**, 16–22 (2005)
73. M.J. Ramsay, W.W. Clark, Proc. SPIE **4332**, 429–438 (2001)
74. R. Sood, Y.B. Jeon, J.H. Jeong, S.G. Kim, in *Tech. Digest 2004 Solid State Sensor Actuator Workshop*, Hilton Head, South Carolina, 2004
75. S. Kim, W.W. Clark, Q.-M. Wang, Proc. SPIE **5055**, 307–318 (2003)